







PRMT5 deficiency in myeloid cells reprograms macrophages to enhance antitumor immunity and synergizes with anti-PD-L1 therapy

Shiyu Chen ^{1,2,3} Zheyi Chen ¹ Bingqian Zhou ¹ Yongyu Chen ¹
Yiren Huang ¹ Jian Cao ^{4,5} Lisong Shen ^{1,2,3} Yingxia Zheng ^{1,2,3}

To cite: Chen S, Chen Z, Zhou B, *et al.* PRMT5 deficiency in myeloid cells reprograms macrophages to enhance antitumor immunity and synergizes with anti-PD-L1 therapy. *Journal for ImmunoTherapy of Cancer* 2025;**13**:e011299. doi:10.1136/jitc-2024-011299

► Additional supplemental material is published online only. To view, please visit the journal online (<https://doi.org/10.1136/jitc-2024-011299>).

Accepted 17 March 2025



© Author(s) (or their employer(s)) 2025. Re-use permitted under CC BY-NC. No commercial re-use. See rights and permissions. Published by BMJ Group.

For numbered affiliations see end of article.

Correspondence to

Dr Yingxia Zheng;
zhengyingxia@xinhuanet.com.cn

Dr Lisong Shen;
lisongshen@hotmail.com

Dr Jian Cao;
jian.cao@rutgers.edu

ABSTRACT

Background Arginine methyltransferase protein arginine methyltransferase 5 (PRMT5) plays a significant role in immune regulation, particularly within the tumor microenvironment (TME). Macrophages are crucial modulators of both innate and adaptive immune responses, and their differentiation into tumor-associated macrophages is critical in shaping the TME. Despite ongoing clinical trials of small molecule inhibitors of PRMT5 for cancer therapy, their effects on macrophages, a key component of the immune system, remain poorly understood.

Methods A pan-cancer single-cell transcriptional analysis was initially conducted to investigate the expression of PRMT5 in tumor-infiltrating myeloid cells. Myeloid-specific deletion of Prmt5 in mice, as well as the use of a PRMT5-specific inhibitor, was performed to evaluate the impact of PRMT5 on macrophage polarization and tumor progression. Bulk and single-cell transcriptomics were employed to explore the mechanistic roles of PRMT5 in regulating lipid metabolism and macrophage polarization. Additionally, the therapeutic potential of combining Prmt5 deletion with anti-programmed death-ligand 1 (PD-L1) therapy was assessed to study its effects on antitumor immunity in vivo.

Results The pan-cancer single-cell transcriptional analysis revealed that PRMT5 is highly expressed in the PPARG-macrophage subset, which correlates with poor patient survival. Myeloid-specific deletion of Prmt5 reprogrammed macrophages towards an antitumor phenotype, effectively inhibiting tumor progression. Mechanistically, PRMT5 was found to regulate lipid metabolism and drive macrophage polarization toward an anti-inflammatory state via the STAT6-PPAR γ pathway, fostering an immunosuppressive TME conducive to tumor growth. Notably, Prmt5 deletion induced PD-L1 expression on myeloid cells. Combining Prmt5 deletion with anti-PD-L1 therapy significantly enhanced antitumor efficacy, demonstrating a synergistic therapeutic effect.

Conclusions These findings uncover a crucial role for PRMT5 in macrophage biology and suggest that targeting PRMT5 in myeloid cells offers a promising new approach for cancer immunotherapy. The combination of PRMT5 inhibition with anti-PD-L1 therapy may provide a potent strategy to reprogram the TME and enhance antitumor immune responses.

WHAT IS ALREADY KNOWN ON THIS TOPIC

⇒ Previous studies have suggested that protein arginine methyltransferase 5 (PRMT5) may be involved in the regulation of immune responses, but its specific role in macrophages and its implications in the tumor microenvironment (TME) were not well understood.

WHAT THIS STUDY ADDS

- ⇒ This study reveals that PRMT5 is highly expressed in a subset of PPARG-macrophages, which correlates with poor patient survival.
- ⇒ Myeloid-specific deletion of Prmt5 reprograms macrophages towards an antitumor phenotype, inhibiting tumor progression.
- ⇒ Mechanistically, PRMT5 regulates lipid metabolism and drives macrophage polarization towards an anti-inflammatory state via the STAT6-PPAR γ pathway.
- ⇒ Notably, Prmt5 deletion induces PD-L1 expression on myeloid cells, and combining Prmt5 deletion with anti-PD-L1 therapy significantly enhances antitumor efficacy.

HOW THIS STUDY MIGHT AFFECT RESEARCH, PRACTICE OR POLICY

- ⇒ This study provides new insights into the role of PRMT5 in macrophage biology, particularly in the context of the TME, and suggests that targeting PRMT5 in myeloid cells could be a promising new approach for cancer immunotherapy.

INTRODUCTION

Protein arginine methyltransferase 5 (PRMT5) is a highly conserved enzyme that catalyzes the symmetric di-methylation of arginine residues on histones and some non-histone proteins. PRMT5 is involved in a variety of cellular processes, including chromatin remodeling, transcriptional regulation, RNA processing, cell proliferation and differentiation.¹ Its diverse effects on RNA metabolism highlight its importance in gene

expression regulation at multiple levels. For example, PRMT5-mediated methylation of the splicing regulator SRSF1 modulates its activity and promotes exon skipping.² Additionally, PRMT5 methylates the RNA-binding protein HNRNPA1, implicated in alternative splicing regulation, messenger RNA (mRNA) stabilization, and translation.³ Furthermore, PRMT5 has been shown to methylate several transcription factors and epigenetic modifiers, including P53, NF- κ B, E2F1, DNMT1, and EZH2, thereby regulating their activity.^{4–8} Dysregulation of PRMT5 activity has been implicated in a variety of human diseases, including neurological disorders such as Alzheimer's disease and multiple sclerosis,^{9–10} as well as cancers like leukemia, lymphoma, lung cancer, and breast cancer.^{2–11–13} Recent research indicated that targeting PRMT5 with small molecule inhibitors holds promise for treating various types of cancer. A number of PRMT5 inhibitors such as PF-06939999 and JNJ-64619178 have been developed and tested in preclinical studies.^{14–15} Moreover, the second-generation PRMT5 inhibitors like AMG193 and MRTX1719 were safe and demonstrated preliminary antitumor activity in patients with solid tumors with methylthioadenosine phosphorylase (MTAP) deficiency.^{16–17}

PRMT5 also plays a critical role in regulating the immune system. Research from our group and others has demonstrated PRMT5's involvement in the differentiation, activation, and function of T and B cells. Specific deletion of *Prmt5* in mouse T cells induces their terminal differentiation and accelerates tumor progression.¹⁸ Conversely, *Prmt5* deletion in B cells increases Ccl22 expression, attracting natural killer (NK) cells to the tumor microenvironment (TME) and delaying tumor progression.¹⁹ These findings suggest that PRMT5 has distinct effects on different immune cell subsets, influencing tumor dynamics in varied ways. However, the impact of PRMT5 inhibition on myeloid cells and their contribution to tumor progression and immune modulation remains unclear.

Macrophages are key immune cells that play critical roles in both innate and adaptive immune responses. They differentiate from circulating monocytes in response to specific signals^{20–21} and are broadly categorized into two main statuses: classically activated macrophages (M1) and alternatively activated macrophages (M2). Tumor-associated macrophages (TAMs) are predominantly skewed towards the M2 phenotype, which promotes tumor progression through angiogenesis, immune suppression, and facilitation of tumor cell invasion and metastasis. Reprogramming TAMs from a protumor M2-like status to an antitumor M1-like status is a major area of interest for developing novel cancer immunotherapies.

In this study, we first analyzed single-cell RNA sequencing (RNA-seq) data of PRMT5 expression from pan-cancer tumor-infiltrating monocyte-macrophage subsets, identifying high PRMT5 expression in the PPARG-macrophage subset. Additionally, macrophages expressing high levels of PRMT5 correlate with poor survival outcomes. We then

employed *Lysm-cre-Prmt5^{fl/fl}* mice and PRMT5-specific inhibitors to elucidate the role of PRMT5 in macrophage polarization and its effects on the TME. Our results demonstrate that *Prmt5* deletion or PRMT5 inhibitor treatment significantly reduces M2 macrophage polarization in vitro, primarily through alterations in cholesterol metabolism via the STAT6-PPAR γ pathway. In vivo allograft models showed that *Prmt5* deletion in myeloid cells reprograms macrophages and induces an antitumor phenotype. Moreover, *Prmt5* deletion in myeloid cells induced programmed death-ligand 1 (PD-L1) expression, and combining PRMT5 inhibition with anti-PD-L1 therapy showed synergistic effects on suppressing tumor growth. Our study unveils PRMT5 as a key regulator of macrophage differentiation and function, highlighting its potential as a therapeutic target not only for directly targeting cancer cells, but also for reshaping the TME to promote an antitumor response.

RESULTS

PRMT5 expressed highly in PPARG-macrophage subset and correlated with poor cancer survival

We first analyzed PRMT5 expression in peripheral blood mononuclear cells (PBMCs) using publicly available data sets. First, single-cell RNA-seq data revealed that monocytes are among the cell types with the high levels of PRMT5 (online supplemental figure 1). Additionally, PRMT5 is upregulated in inflammatory macrophages compared with monocytes (online supplemental figure 1B), based on a separate microarray data set (GSE5099). In mouse allograft colorectal cancer models of MC38, we observed significantly higher PRMT5 expression in TAMs compared with spleen macrophages (figure 1A). Multicolor immunofluorescence analysis of human colorectal cancer tissue further confirmed elevated PRMT5 expression in CD206+ macrophages compared with CD206– macrophage (figure 1B). Furthermore, we analyzed PRMT5 expression in infiltrating monocyte-derived macrophage subsets across various cancers, including lung, liver, breast, colorectal, renal, and esophageal cancers from publicly available pan-cancer single-cell transcriptomic data (GSE154763). Interestingly, analysis revealed that PRMT5 is most highly expressed in PPARG+tumor-infiltrating macrophages, which co-express MRC1 (CD206) (figure 1C), indicating that these cells constitute an M2-related macrophage genes. Moreover, PPARG+macrophages from tumor tissue expressed higher levels of PRMT5 than those from normal tissue (figure 1D). We then examined the relationship between PRMT5 expression in tumor-infiltrating macrophages and survival outcomes across six cancer types (lung adenocarcinoma, colorectal cancer, head and neck cancer, breast cancer, liver cancer, and skin cancer) using the GEPIA database (<http://gepia2.cancer-pku.cn/>). Higher PRMT5 expression in macrophages correlates with shorter survival times in patients with cancer (figure 1E and online supplemental figure 1C). These

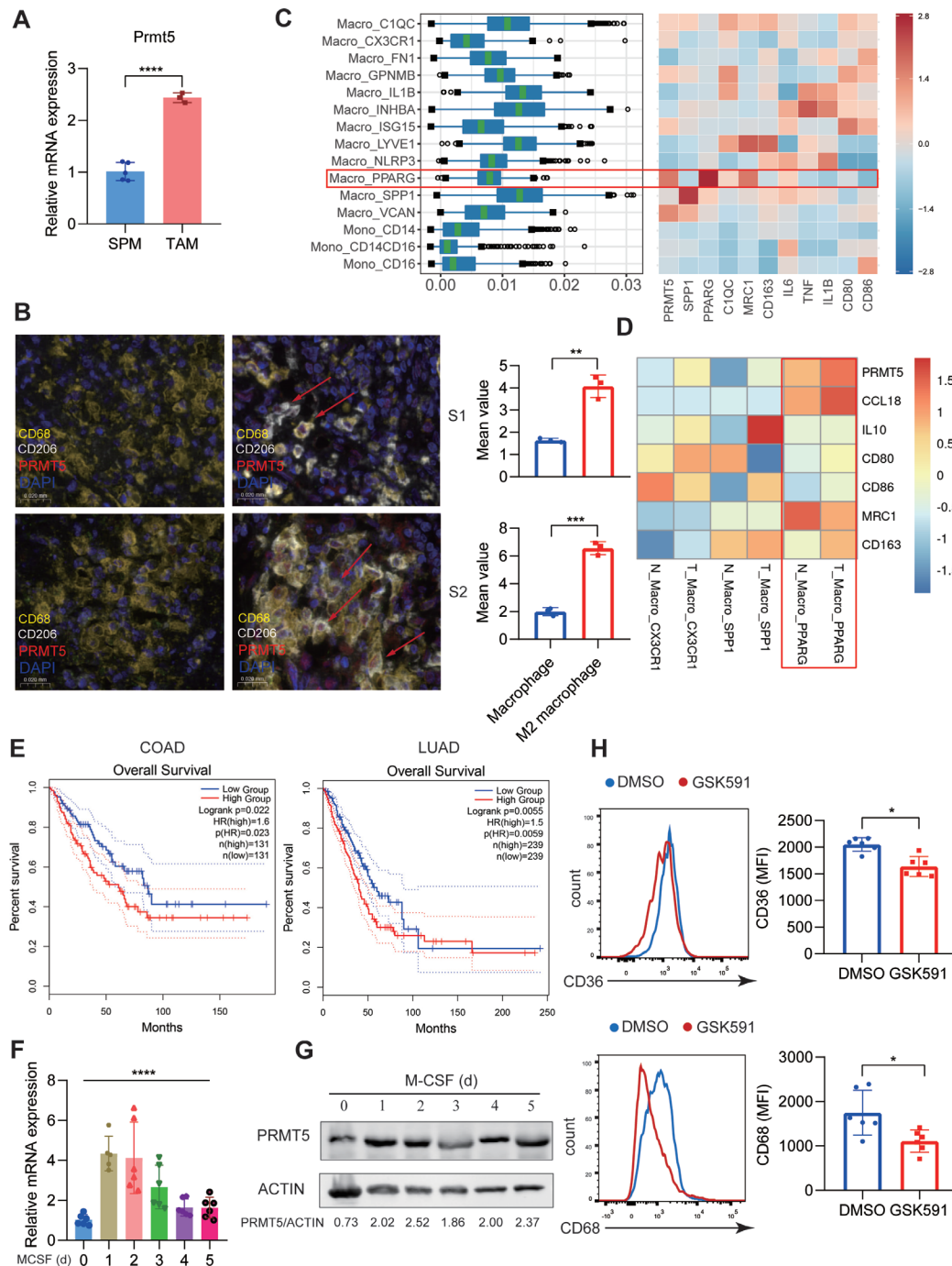


Figure 1 PRMT5 expressed highly in macrophages and was involved in the monocyte-to-macrophage differentiation process. (A) Spleen macrophage (SPM) and tumor-associated macrophage (TAM) were isolated from MC38 tumor-bearing C57BL/6 mice (n=3), *Prmt5* expression was determined by qPCR. (B) PRMT5, CD68, CD206 expression in human colorectal tissue by multicolor IHC staining was measured. Representative data from two patients were shown. (C) PRMT5 and related genes in macrophage subpopulations across 15 types of tumors were analyzed from pan-cancer single-cell transcriptomic data (GSE154763). (D) PRMT5 expression in distinct subsets of tumor-infiltrating macrophages and the corresponding subsets in normal tissues from pan-cancer single-cell transcriptomic data. (E) The relationship of PRMT5 expression levels in tumor-infiltrating macrophages and survival outcomes in colorectal cancer (COAD) and lung adenocarcinoma (LUAD) using the (<http://gepia2.cancer-pku.cn/>) database website. (F, G) Monocytes isolated from human PBMC were stimulated with M-CSF for different times. PRMT5 mRNA expression was measured by qPCR (F) (n=5–6); PRMT5 protein expression was measured by western blot (G); the data represented from the two experiments were shown. (H) Monocytes isolated from human PBMC were stimulated with M-CSF and treated with GSK591 or DMSO, CD68 and CD36 expression were measured by flow cytometry (n=6). The mean±SD's was graphed. Statistical differences were determined by one-way analysis of variance (F) or the two-tailed unpaired Student's t-test (A, B, H), *p<0.05, **p<0.01, ***p<0.001, ****p<0.0001. IHC, Immunohistochemistry; M-CSF, macrophage colony-stimulating factor; MFI, Mean Fluorescence Intensity; mRNA, messenger RNA; PBMC, peripheral blood mononuclear cell; PRMT5, protein arginine methyltransferase 5; qPCR, quantitative PCR.

data suggested that PRMT5 may be involved in macrophage differentiation, and play a critical role in the function of TAM.

To further validate these findings, we isolated human monocytes from healthy donors and stimulated them with macrophage colony-stimulating factor (M-CSF) to induce macrophages. Under M-CSF stimulation, PRMT5 expression was upregulated at both mRNA and protein levels with a surge at mRNA levels at day 1. However, the levels of transcription and protein increase are not temporally consistent (figure 1F,G). Treatment with PRMT5-specific inhibitor GSK591 at the onset of culture reduced PRMT5 activity, as evidenced by decreased dimethyl symmetric arginine (SDMA) level (online supplemental figure 1D). The treatment also reduced the expression of macrophage-related genes like CD36 and CD68 (figure 1H). These in vitro findings support the role of PRMT5 in macrophage differentiation.

Prmt5 deletion impaired the macrophage differentiation and migration

To further determine whether PRMT5 similarly impacts monocyte differentiation in mice, we isolated mouse bone marrow monocytes and cultured them with M-CSF. Consistently, *Prmt5* expression is upregulated when mouse monocytes are stimulated with M-CSF (figure 2A). To assess the role of PRMT5 in monocyte-macrophage differentiation in vivo, we crossed *Lysm-cre* transgenic mice with *Prmt5^{fl/fl}* mice to generate *Lysm-cre-Prmt5^{fl/fl}* conditional knockout mice (*Prmt5* cKO) (figure 2B). *Prmt5* mRNA expression in bone marrow-derived macrophages (BMDMs) of *Prmt5* cKO mice was significantly reduced compared with their wild type littermates, confirming the successful construction of the cKO model (figure 2C).

We then examined the phenotype of *Prmt5* cKO mice. Analysis of CD11b+myeloid cells and monocytes in the bone marrow showed no significant differences between *Prmt5* cKO and control groups (online supplemental figure 2A, B). Meanwhile, percentages of CD11b+myeloid cells and dendritic cells (DC) in spleens showed no differences between *Prmt5* cKO and control groups (online supplemental figure 2C, D). However, we observed a decreased frequency of monocytes (CD11b+Ly-6C+Ly6G⁻) and macrophages (F4/80+) in the spleens and peritoneal cavities of *Prmt5* cKO mice, compared with controls (figure 2D–F). No significant difference between the two groups was observed on neutrophils, T and B cells (online supplemental figure 2E–G).

CCL2 has been reported to interact with CCR2 on mono/macrophages, mediating their migration to sites of immune response.²² We found a significant decrease in CCR2 expression in Ly6C+cells from the blood of *Prmt5* cKO mice compared with control mice (figure 2G). To further investigate macrophage recruitment and migration, we induced peritonitis in mice using thioglycolate.^{23, 24} 3 days post-injection, the percentage of CD11b+cells in the peritoneal cavity was significantly lower in *Prmt5* cKO mice compared with controls,

suggesting impaired myeloid cell migration (figure 2H). Moreover, both the percentage and absolute number of macrophages in the peritoneal lavage fluid were significantly lower in *Prmt5* cKO mice compared with controls (figure 2I,J). However, no differences in apoptosis or proliferation were observed in peritoneal macrophages between the two groups (online supplemental figure 2H, I), suggesting that the reduction in macrophages within the peritoneal cavity was primarily due to impaired myeloid cell migration.

PRMT5 promotes macrophage polarization towards the M2 phenotype

We further investigated the role of PRMT5 in macrophage polarization. BMDMs were isolated from *Prmt5* cKO and control mice and stimulated towards either M1 or M2 polarization for 48 hours. Interestingly, while M1-associated genes such as *Il6*, *Tnf*, and *Inos* showed no significant differences between the two groups, the co-stimulatory molecule CD80 was significantly upregulated in *Prmt5* cKO mice (figure 3A and online supplemental figure 3A). Conversely, M2-related genes *Arg1*, *Ym1*, and *Mrc1* were significantly downregulated in *Prmt5* cKO mice, correlating with lower CD206 expression as measured by flow cytometry (figure 3B,C). Moreover, SDMA levels were significantly reduced in the M2 inducing system in *Prmt5* cKO mice (figure 3D) compared with the control mice, suggesting that PRMT5 plays a more prominent role in M2 differentiation than M1 differentiation.

To further explore this, PRMT5-specific inhibitor GSK591 was applied in the M1/M2 polarization experiments. We generated three types of macrophages—mouse BMDMs, THP-1-derived macrophages, and human Mo-macs. Cells were treated with or without GSK591 for 2 days, followed by stimulation with specific cytokines to induce M1 or M2 polarization (online supplemental figure 3B). Consistently, GSK591 treatment during BMDM polarization significantly increased CD80 expression, but not other M1-related molecules such as *Tnf* and *Inos* (figure 3E and online supplemental figure 3C). M2-related genes *Arg1*, *Ym1*, and *Mrc1* were significantly downregulated in GSK591-treated M2-polarized macrophages, with reduced CD206 expression confirmed by flow cytometry (figure 3F,G). Additionally, human Mo-macs isolated from healthy donors and treated with GSK591 during M1 and M2 polarization exhibited downregulated CD206 and CCL18 expressions in M2-polarized macrophages, while M1-related genes were unaffected (figure 3H and online supplemental figure 3D). Similarly, THP-1 cells stimulated into macrophages with PMA (Phorbol 12 - Myristate 13 - Acetate) and then polarized into M1 or M2 showed that GSK591 treatment reduced the expression of M2-related markers without affecting M1-related genes (online supplemental figure 3E, F). These findings indicate that PRMT5 is essential for macrophage polarization towards the M2 phenotype.

To further examine whether the function of macrophages was altered after knockdown of PRMT5, first,

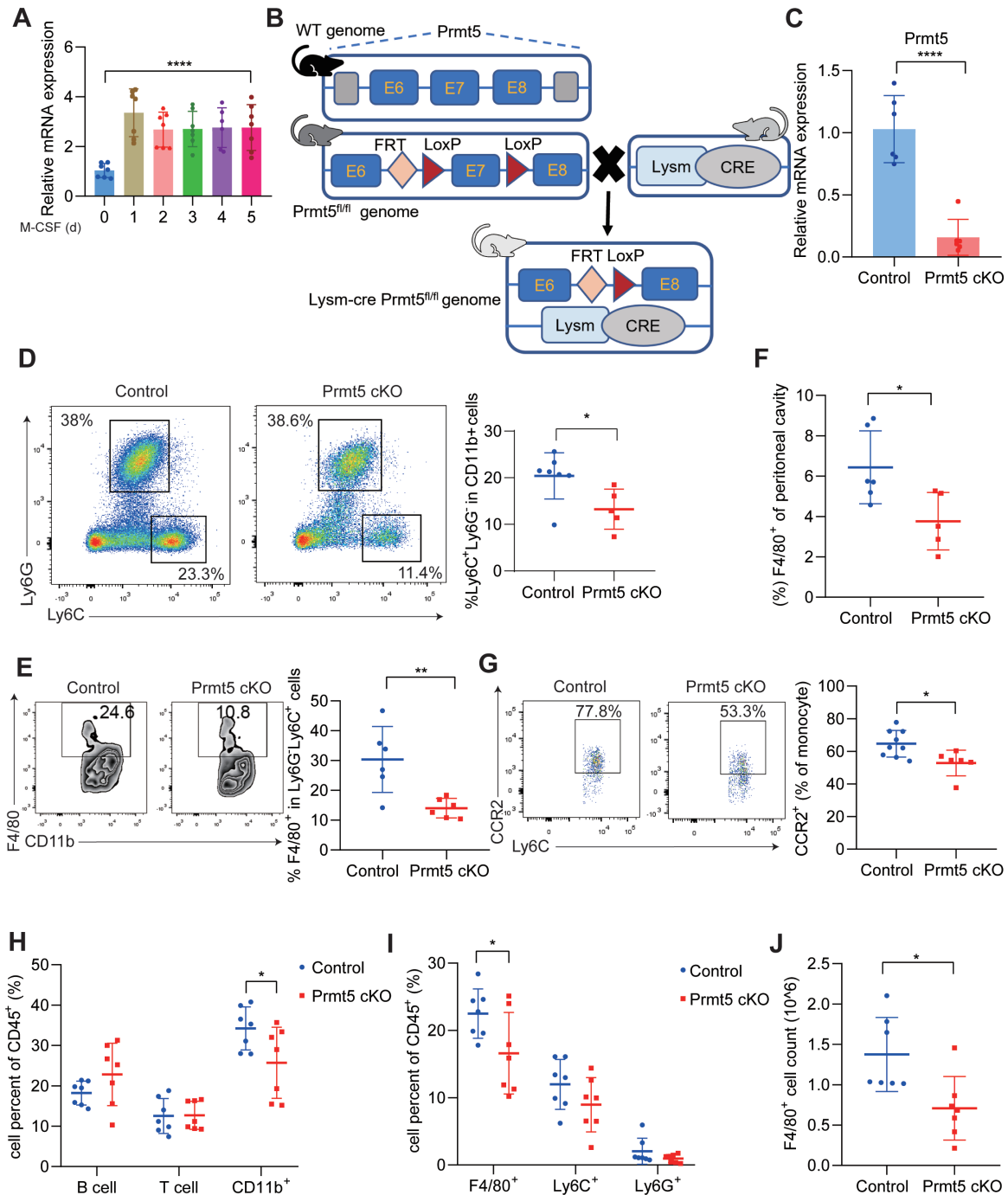


Figure 2 PRMT5 regulates macrophage differentiation and migration. (A) Bone marrow monocytes were isolated from C57BL/6 (n=6–7) and stimulated with M-CSF with differentiation time, *Prmt5* expression was determined by qPCR. (B) Schematic of *Prmt5* genomic locus targeting strategy from the European Conditional Mouse Mutagenesis Program. Exon 7 of *Prmt5* was flanked by loxP sites and then crossed with Lysm-Cre mice to produce *Lysm-cre-Prmt5*^{fl/fl} mice (*Prmt5* cKO) and littermate control mice. (C) BMDMs isolated from *Prmt5* cKO and control mice, *Prmt5* expression was measured by real-time qPCR (n=6). (D) Flow cytometry analysis of Ly6C⁺Ly6G⁻ monocytes in control (n=7) and *Prmt5* cKO mice (n=5). The mean±SD was graphed. (E) The frequencies of CD11b⁺F4/80⁺ cells gated in Ly6C⁺Ly6G⁻ cells from control (n=6) and *Prmt5* cKO (n=6) mouse spleens. (F) The frequencies of CD11b⁺F4/80⁺ cells from control (n=6) and *Prmt5* cKO (n=5) mouse peritoneal cavity. (G) The frequencies of CCR2 expression in Ly6C⁺ cells from control (n=9) and *Prmt5* cKO (n=6) mouse blood. (H–J) Control (n=7) and *Prmt5* cKO mice (n=7) were injected with thioglycolate for 3 days, the percentages of B cells, T cells and CD11b⁺ myeloid cells in CD45⁺ cells were determined by flow cytometry (H); the percentages of F4/80⁺ macrophages, Ly6C⁺ monocytes and Ly6G⁺ neutrophils in peritoneal cavity (I); absolute cell number of macrophages in peritoneal cavity (J). The mean±SD was graphed. Statistical differences were determined by one-way analysis of variance (A) or the two-tailed unpaired Student's t-test (C–J), *p < 0.05, **p < 0.01, ****p < 0.0001. cKO, conditional knockout; BMDM, bone marrow-derived macrophages; FACS, Fluorescence - activated Cell Sorting; M-CSF, macrophage colony-stimulating factor; PRMT5, protein arginine methyltransferase 5; qPCR, quantitative PCR.

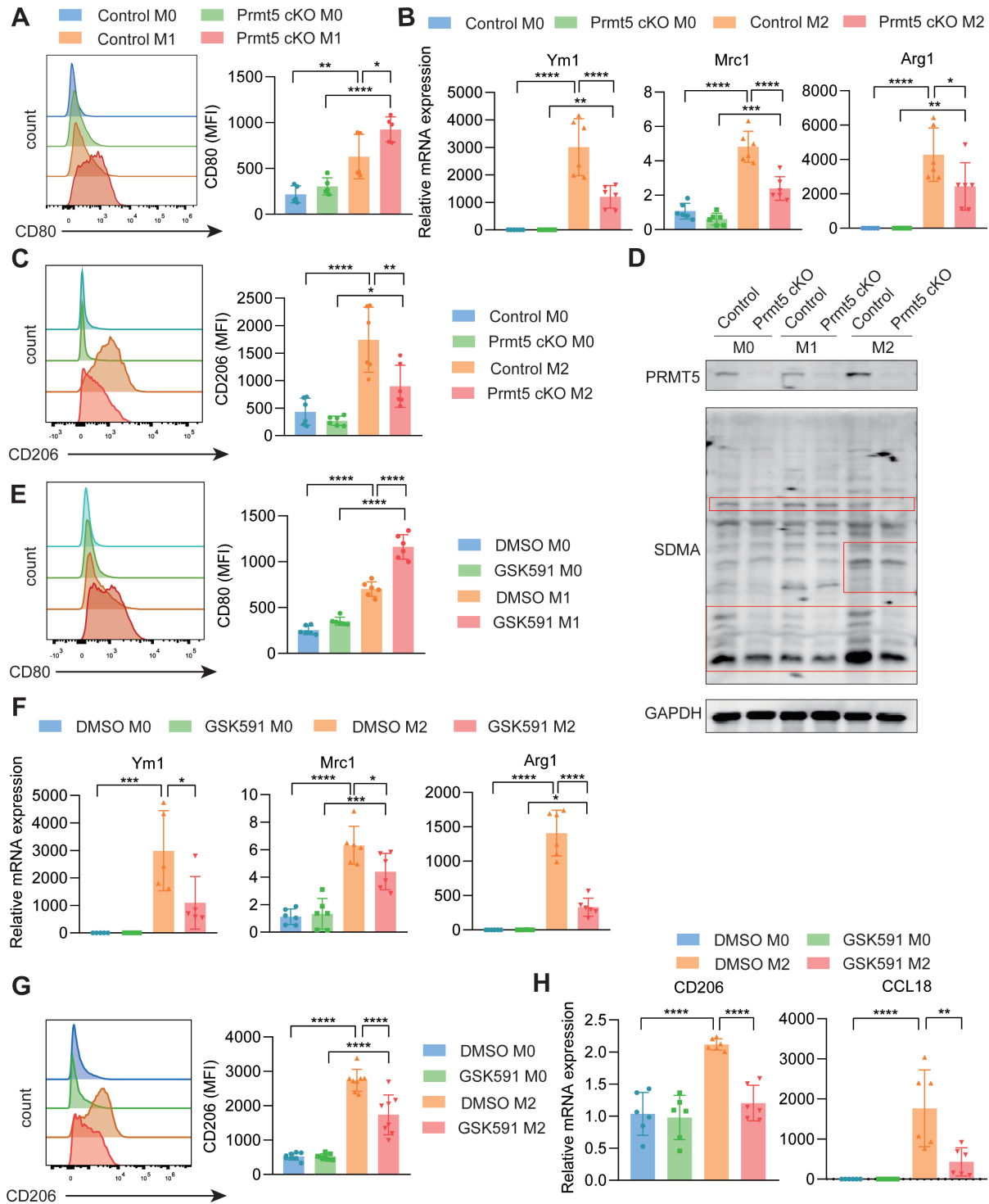


Figure 3 Prmt5 promotes macrophage polarization towards the M2 phenotype. (A–D) Bone marrow cells were isolated from Prmt5 cKO and control mice, then induced to differentiate into macrophages and subsequently stimulated towards M1 or M2 polarization. CD80 expression was assessed by flow cytometry (A); M2 markers including Arg1, Ym1, Mrc1 expressions were measured by real-time qPCR (B); CD206 expression was measured by flow cytometry (C); Prmt5 and SDMA expression were determined by western blot. The data represented from the two experiments were shown (D). (E–G) Bone marrow-derived macrophages isolated from C57BL/6 mice were stimulated towards M1 or M2 polarization treated with DMSO or GSK591. CD80 expression was assessed by flow cytometry (E); M2 markers including Arg1, Ym1, and Mrc1 expressions were measured by real-time qPCR (F); CD206 expression was measured by flow cytometry (G). (H) Human monocyte-derived macrophages from healthy donors' blood treated with GSK591 during M1 and M2 polarization, CD206 and CCL18 expressions were measured by real-time qPCR. The mean±SD was graphed. Statistical differences were determined by one-way analysis of variance, * $p < 0.05$, ** $p < 0.01$, *** $p < 0.001$, **** $p < 0.0001$. cKO, conditional knockout; mRNA, messenger RNA; MFI, Mean Fluorescence Intensity; PRMT5, protein arginine methyltransferase 5; qPCR, quantitative PCR; SDMA, dimethyl symmetric arginine.

we established a macrophage-T cell co-culture system. We found that the proportion of naïve T cells, central memory T cells and Tregs (Regulatory T cells) showed no significant difference between the control and Prmt5 cKO group, while effector memory T cells were elevated in the Prmt5 cKO group (online supplemental figure 4A–D). Meanwhile, reducing PRMT5 expression in BMDMs had little effect on T-cell cytotoxicity, since the expression of interferon (IFN)- γ and tumor necrosis factor (TNF)- α in T cells showed no significant difference between the two groups (online supplemental figure 4E,F). To further investigate the impact of macrophages on tumor cells, we established a co-culture system of BMDMs and MC38 cells in transwell chambers for 3 days and found that control M2 macrophages promote MC38 cell proliferation, compared with M0 macrophages, while no significant difference was exhibited in M0 and M2 BMDMs from the Prmt5 cKO group (online supplemental figure 4G).

Prmt5 regulates lipid metabolism in BMDMs and promotes M2 polarization via the pSTAT6/PPAR γ axis

To further investigate the mechanism by which Prmt5 regulates macrophage polarization, we performed RNA-seq with BMDMs isolated from Prmt5 cKO and control mice. Transcriptomic analysis revealed 1146 upregulated and 166 downregulated genes in Prmt5 cKO BMDMs (online supplemental figure 5A), indicating a role for Prmt5 in gene transcriptional repression, consistent with previous reports.^{4 25 26} Gene Set Enrichment Analysis (GSEA) demonstrated that the downregulated genes were enriched in lipid metabolism pathways, including PPAR signaling, arachidonic acid metabolism, linolenic acid metabolism, arginine biosynthesis (online supplemental figure 5B,C), all of which are associated with M2 differentiation.²⁷

Next, we stimulated BMDMs toward M2 differentiation and performed RNA-seq. In this context, 643 genes were upregulated while 318 genes were downregulated in Prmt5 cKO BMDMs compared with controls (figure 4A). GSEA indicated that the downregulated genes were enriched in cholesterol metabolism pathways (figure 4B,C). Additionally, we used the STRING database to investigate the gene regulatory networks of differentially expressed genes of control and Prmt5 cKO M2 BMDMs. As a result, we found that genes related to macrophage polarization and lipid metabolism were included, such as *Chil3*, *Csf1*, *Tnf*, *Cd80*, *Apoe*. Besides, chemokines and chemokine receptors, such as *Cxcr6*, *Cxcl14*, *Ccr3*, were also involved in the regulatory network (online supplemental figure 5D). A heat map further highlighted that M2-related genes, including *Mrc1*, *Chil3*, *Csf1*, and *Pparg*, were downregulated in Prmt5 cKO M2 BMDMs (figure 4D). Lipid and cholesterol metabolism are key regulators of macrophage activation and function. ATP binding cassette subfamily A member 1 (*Abca1*) and subfamily G member 1 (*Abcg1*) are crucial genes involved in cholesterol efflux and cholesterol metabolism, along with PPAR- γ .²⁸ We analyzed the expression of these genes in our RNA-seq

analysis of M2 BMDMs from control and Prmt5 cKO mice. Consistently, cholesterol metabolism-related genes, including *Abca1*, *Abcg1*, *Eepd1*, *Cyp27a1*, and *Scd1*, were significantly reduced in Prmt5 cKO BMDMs (figure 4E). We verified the downregulation of these genes by quantitative PCR (qPCR) in both Prmt5 cKO M2 BMDMs and GSK591-treated M2 BMDMs (figure 4F,G). These results indicated that Prmt5 regulates lipid metabolism during M2 differentiation.

PPAR γ has been reported to promote M2 polarization through lipid metabolism, which is essential for TAM protumor activation.^{29–31} We verified the expression of PPAR γ using RT-PCR (Reverse Transcription - Polymerase Chain Reaction) and western blot, confirming that its expression was indeed decreased in the Prmt5 cKO group (figure 4H,I). Similarly, GSK591 treatment led to a significantly decreased PPAR γ expression at both the transcriptional and protein levels (figure 4J,K). Moreover, the M2-related ARG1 was downregulated in response to Prmt5 deletion or inhibition (figure 4L,K). It has been reported that the pSTAT6/PPAR γ signaling pathway is involved in M2 polarization.³² We first observed that p-STAT6 was downregulated in M2-polarized BMDMs from Prmt5 cKO mice compared with control mice (figure 4L). Consistent with this, STAT6 phosphorylation was decreased in GSK591-treated BMDMs, human Mo-macs, and THP-1-derived macrophages (figure 4M,N and online supplemental figure 5E). Moreover, suppressor of cytokine signaling 1 (SOCS1), the transcription factor which is a negative regulator of phosphorylation of STAT6³³ was also detected. Data showed that SOCS1 expression was upregulated on interleukin (IL)-4 and IL-13 stimulation, while Prmt5 cKO BMDMs displayed higher SOCS1 expression levels than the control group (online supplemental figure 5F, G). Additionally, we analyzed RNA-seq data from the TCGA (The Cancer Genome Atlas) database to explore the relationship between the expression of PRMT5 and PPARG or STAT6 in tumor-infiltrating macrophages. The analysis revealed a positive correlation between PRMT5 and both PPARG and STAT6 expression across several tumor types, such as Lung Adenocarcinoma (LUAD) and colorectal cancer (figure 4O,P). These findings suggest that PRMT5 promotes macrophage M2 polarization by regulating cholesterol metabolic reprogramming through PPAR γ expression.

Myeloid cell-specific deletion of Prmt5 inhibits tumor progression

Our previous study indicated that Prmt5 promotes M2 macrophage differentiation in vitro (figure 3). To investigate the impact of myeloid cell-specific deletion of Prmt5 on tumor development, we implanted syngeneic MC38 colorectal cancer cells subcutaneously into Prmt5 cKO mice and littermate controls. As expected, Prmt5 cKO mice developed smaller tumors than the control group (figure 5A,B). We analyzed the tumor-infiltrating CD45+ immune cells, using the gating strategy shown in online supplemental figure 6A, B. No significant

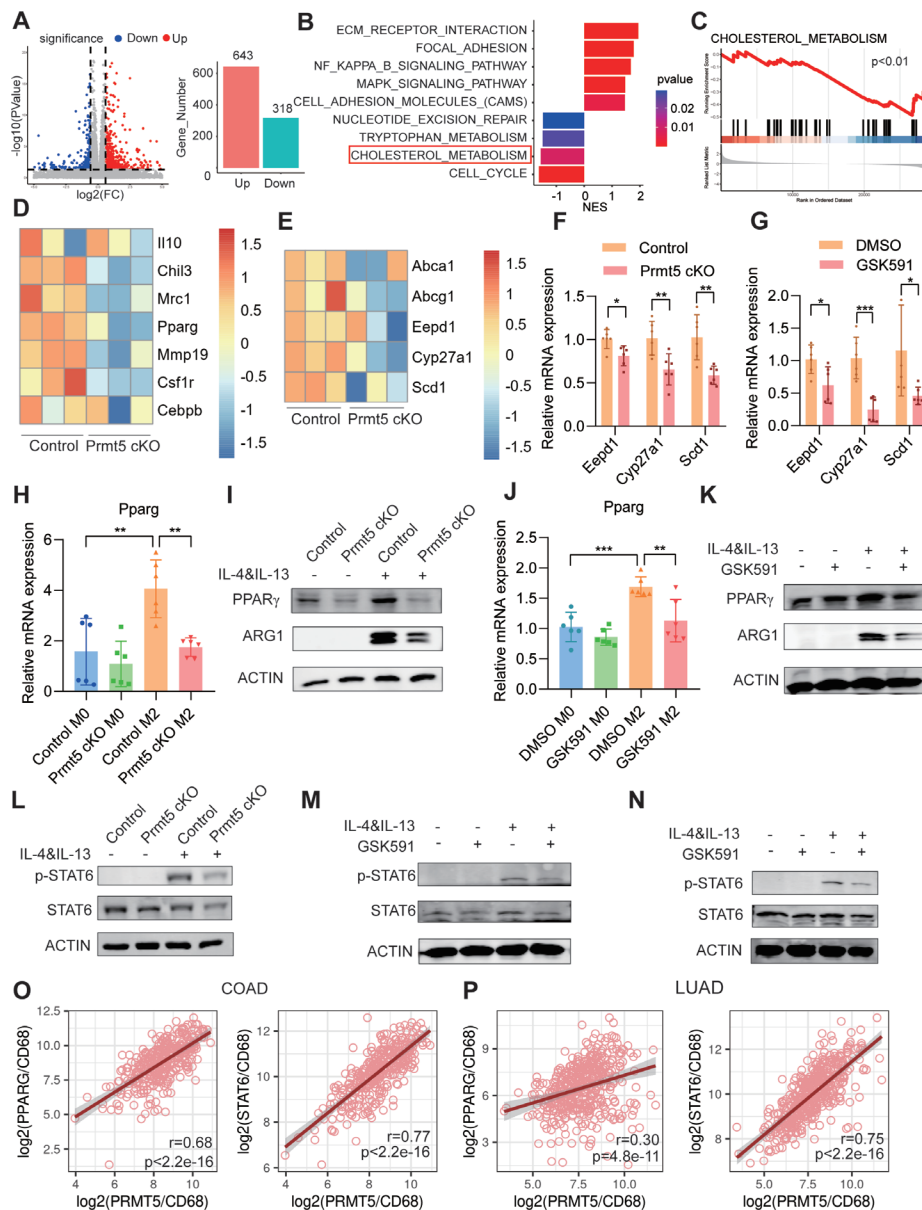


Figure 4 Prmt5 regulates lipid metabolism in BMDMs and promotes M2 polarization through the pSTAT6–PPAR γ axis. Bone marrow cells were isolated from Prmt5 cKO and control mice, then induced to differentiate into macrophages and polarized into M2 phenotype, then for RNA sequencing. (A) Volcano plot showing the upregulated and downregulated genes in M2 BMDMs between two groups. (B) M2 BMDMs gene expression profiles were analyzed by Gene Set Enrichment Analysis, upregulated and downregulated pathways were shown by the normalized enrichment score. (C) Enrichment plots of cholesterol processes in M2 BMDMs between the two groups. (D) Heatmap of M2-related gene expression in M2 BMDMs from control and Prmt5 cKO mice. (E) Heatmap of genes associated with cholesterol metabolism in M2 BMDMs from control and Prmt5 cKO mice. (F) Eepd1, Cyp27a1 and Scd1 expression in M2 BMDMs from control and Prmt5 cKO mice by qPCR. (G) M2 BMDMs were induced from C57BL/6 mice, and treated with GSK591 or DMSO; Eepd1, Cyp27a1 and Scd1 expression were measured by qPCR. (H, I) M2 BMDMs were induced from control and Prmt5 cKO mice, Pparg expression was measured by qPCR (H); PPAR γ and ARG1 expression were measured by western blot (I). (J, K) M2 BMDMs were induced from C57BL/6 mice, and treated with GSK591 or DMSO; Pparg expression was measured by qPCR (J); PPAR γ and ARG1 expression were measured by western blot (K). (L) BMDMs were generated from control and Prmt5 cKO mice and stimulated with IL-4 and IL-13 for 12 hours, p-STAT6 expression was measured by western blot. (M) BMDMs were generated from C57/BL6 mice and stimulated with IL-4 and IL-13 for 12 hours treated with GSK591 or DMSO, p-STAT6 expression was measured by western blot. (N) Human Mo-macs from healthy donors' blood treated with GSK591 and stimulated with IL-4 and IL-13 for 12 hours, p-STAT6 expression were measured by western blot. (O–P) TCGA database to analyze the correlation between PRMT5 and PPARG expression, PRMT5 and STAT6 expression in colorectal cancer (COAD) (O) and lung adenocarcinoma (LUAD) (P). The mean \pm SD was graphed. Statistical differences were determined by unpaired Student's t-test (F, G) or one-way analysis of variance (H, J), * p <0.05, ** p <0.01, *** p <0.001. One of the three similar representative data was shown. BMDM, bone marrow-derived macrophages; cKO, conditional knockout; IL, interleukin; mRNA, messenger RNA; PRMT5, protein arginine methyltransferase 5; qPCR, quantitative PCR; TCGA, The Cancer Genome Atlas.

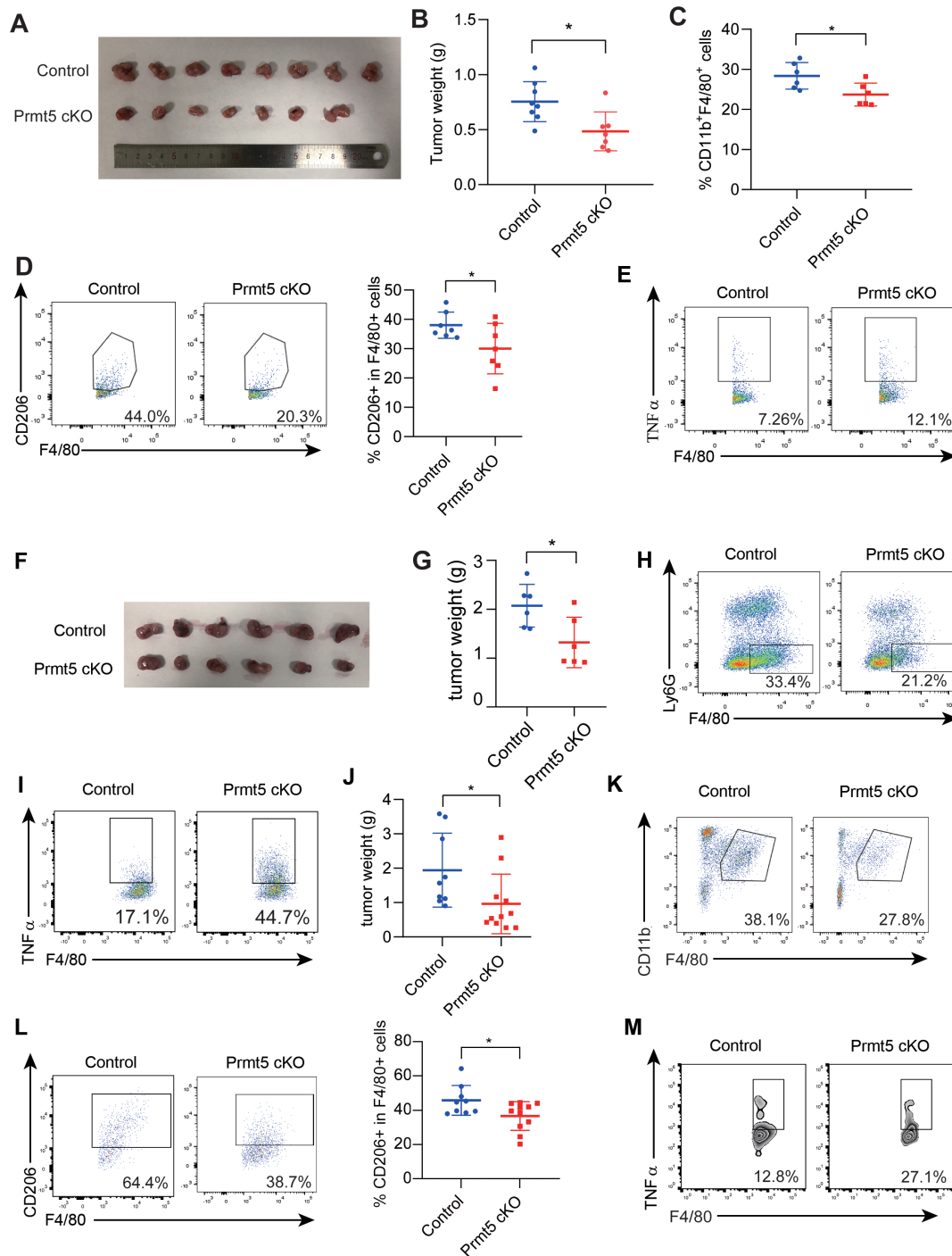


Figure 5 Myeloid cell-specific deletion of Prmt5 protected tumor progression. (A–B) MC38 cancer cells were s.c. implanted into Prmt5 cKO (n=7) and littermate control mice (n=8), images of resected tumors (A) and tumor weights (B) in the two groups were shown. (C) The frequency of CD11b⁺F4/80⁺TAM cells from Prmt5 cKO (n=6) and control (n=6) was determined by flow cytometry. (D) The frequency of CD206⁺ cells in F4/80⁺TAM from Prmt5 cKO (n=7) and control (n=7) was determined by flow cytometry. (E) The frequency of TNF-α⁺ cells in F4/80⁺TAM from Prmt5 cKO (n=7) and control (n=7) was determined by flow cytometry. (F–I) LLC cancer cells were s.c. implanted into Prmt5 cKO (n=6) and littermate control mice (n=6), image of resected tumors (F) and tumor weights (G) in the two groups were shown. (H) The frequency of CD11b⁺F4/80⁺TAM cells from Prmt5 cKO and control was determined by flow cytometry. (I) The frequency of TNF-α⁺ cells in F4/80⁺TAM from Prmt5 cKO and control was determined by flow cytometry. (J–M) B16 cancer cells were s.c. implanted into Prmt5 cKO (n=11) and littermate control mice (n=9). (J) Tumor weights in the two groups were shown. (K) The frequency of CD11b⁺F4/80⁺TAM cells from Prmt5 cKO and control was determined by flow cytometry. (L) The frequency of CD206⁺ cells in F4/80⁺TAM cells from Prmt5 cKO (n=11) and control (n=9) was determined by flow cytometry. (M) The frequency of TNF-α⁺ cells in F4/80⁺TAM cells from Prmt5 cKO and control was determined by flow cytometry. The mean±SD was graphed. Statistical differences were determined by Student's t-test, *p<0.05, **p<0.01. cKO, conditional knockout; PRMT5, protein arginine methyltransferase 5; s.c, subcutaneous Injection; TAM, tumor-associated macrophage; TNF, tumor necrosis factor.

differences were observed in the proportions of CD3+T cells, NK cells, or CD4+Foxp3+ Treg cells between the two groups (online supplemental figure 6C, D). However, we observed a decrease of macrophages and an increase in neutrophils in the tumor tissue of Prmt5 cKO mice (figure 5C and online supplemental figure 6E). Additionally, CD206 expression was decreased in Prmt5 cKO macrophages (figure 5D), while TNF- α expression was elevated (figure 5E and online supplemental figure 6F), suggesting that the reduction of M2 macrophages in Prmt5 cKO tumors may contribute to the inhibition of tumor progression. We further found reducing CCR2 expression in macrophages from the Prmt5 cKO group (online supplemental figure 6G). Moreover, we implanted syngeneic LLC (Lewis Lung Carcinoma) lung cancer cells subcutaneously into Prmt5 cKO mice and their littermate controls. Consistent with the MC38 tumor models, Prmt5 cKO in host suppressed tumor growth compared with the control hosts (figure 5F,G), and the percentage of TAMs was also reduced (figure 5H and online supplemental figure 6H) while TNF- α expression was elevated in Prmt5 cKO macrophages (figure 5I and online supplemental figure 6I). Regarding T cells, neutrophils and monocytes showed no significant changes between the two groups (online supplemental figure 6J). To further validate these findings, we used another mouse tumor model B16, and found that Prmt5 cKO mice developed smaller tumors than the control group (online supplemental figure 6K and figure 5J). Consistent with previous findings, we observed a decrease of F4/80+macrophages in Prmt5 cKO mice (figure 5K and online supplemental figure 6L). Additionally, CD206 expression was decreased in Prmt5 cKO macrophages (figure 5L). And TNF- α expression had a trend of increase in Prmt5 cKO macrophages (figure 5M and online supplemental figure 6M), while tumor-bearing Prmt5 cKO mice exhibited an increase in T cells (online supplemental figure 6N). These data indicated that despite the distinct immune microenvironments across different tumor types, prmt5 deficiency in macrophages consistently reprograms macrophages toward an antitumor phenotype and showed a consistent trend of tumor reduction.

Prmt5 deficiency in myeloid cells reprograms macrophages and induces an antitumor phenotype in Prmt5 cKO mice

To access the impact of myeloid cell-specific deletion of Prmt5 on the immune landscape of the TME, we performed single-cell RNA-seq of CD45+immune cells infiltrating tumors in Prmt5 cKO and control mice. We revealed major immune cell subsets, including T cells, B cells, monocytes/macrophages, neutrophils, DCs, and NK cells (figure 6A and online supplemental figure 7A). In tumors from Prmt5 cKO mice, the proportion of infiltrating neutrophils and DCs increased, while the proportion of monocytes/macrophages decreased; however, the proportions of NK cells, B cells, and T cells remained unchanged, consistent with the flow cytometry results (figure 6B). To further analyze the monocyte-macrophage

population, we performed unsupervised clustering on these cells and identified six clusters: Arg1-Macro, Pparg-Macro, Tnf-Macro, C1qc-Macro, Mki67-Macro and Ccr2-Mono (figure 6C). The corresponding marker genes were shown (figure 6D). GSEA revealed that the Tnf-Macro subset was enriched for M1-related genes, compared with other macrophage/monocyte subsets (figure 6E). Enrichment analysis revealed that the Pparg-Macro cluster was enriched in pathways related to negative regulation of immune system processes, suggesting the inflammatory modulation of this subset (figure 6F). Notably, Prmt5 cKO mice showed significant decreases in the Pparg-Macro and Mki-67-Macro subsets, alongside increases in the Tnf-Macro and C1qc-Macro subsets (figure 6G). M2-related genes, including *Chil3*, *Ctsc*, and *Csf1r*, were downregulated in TAMs from Prmt5 cKO mice compared with control mice, while the M1-related genes, such as *Tnf* and *Cd86*, were upregulated (figure 6H). Similarly, the expression of monocyte-macrophage migration receptor genes *Ccr2* was downregulated (figure 6H). Conversely, chemokines *Cxcl2*, *Ccl2*, and *Ccl5* were upregulated in Prmt5 cKO mice, with these chemokines being highly expressed in Tnf-Macrophages, potentially promoting neutrophil migration consistent with the increased proportion of neutrophils observed in Prmt5 cKO mice (figure 6H,I). Importantly, KEGG (Kyoto Encyclopedia of Genes and Genomes) enrichment analysis revealed that the TNF signaling pathway, Fc gamma R-mediated phagocytosis, and antigen processing and presentation were all enriched in neutrophils (figure 6J), suggesting an antitumor phenotype of the infiltrating neutrophils.³⁴ We further re-clustered T cells into ten subtypes, including naïve and activated T cells, Treg cells, and Th17 cells (online supplemental figure 7B). The proportions of T-cell subclusters showed no significant difference between control and Prmt5 cKO mice (online supplemental figure 7C). Additionally, there were not significant differences in *Gzmb* expression or cytotoxic score in the CD8+T cells between the two groups (online supplemental figure 7D, E), suggesting that myeloid cell-specific deletion of Prmt5 may not directly impact T cells function in the TME. Lastly, we assessed NOS2 expression, a marker of the pro-inflammatory phenotype of macrophages.³⁵ Flow cytometry analysis revealed a significantly increase in NOS2+macrophages in TAMs of Prmt5 cKO mice (figure 6K). Moreover, real-time RT-PCR showed a decrease in PPAR γ expression in TAM isolated from Prmt5 cKO mice compared with control mice (figure 6L). Our results indicate that Prmt5 deficiency in myeloid cells reprograms macrophages and induces an antitumor phenotype in the TME.

Anti-PD-L1 exhibits enhanced antitumor potency in Prmt5 cKO mice

Our previous study demonstrated that Prmt5 inhibition induces PD-L1 expression in lung cancer, thereby potentially suppressing T cell-mediated antitumor immune responses.³⁶ We questioned whether the deletion of

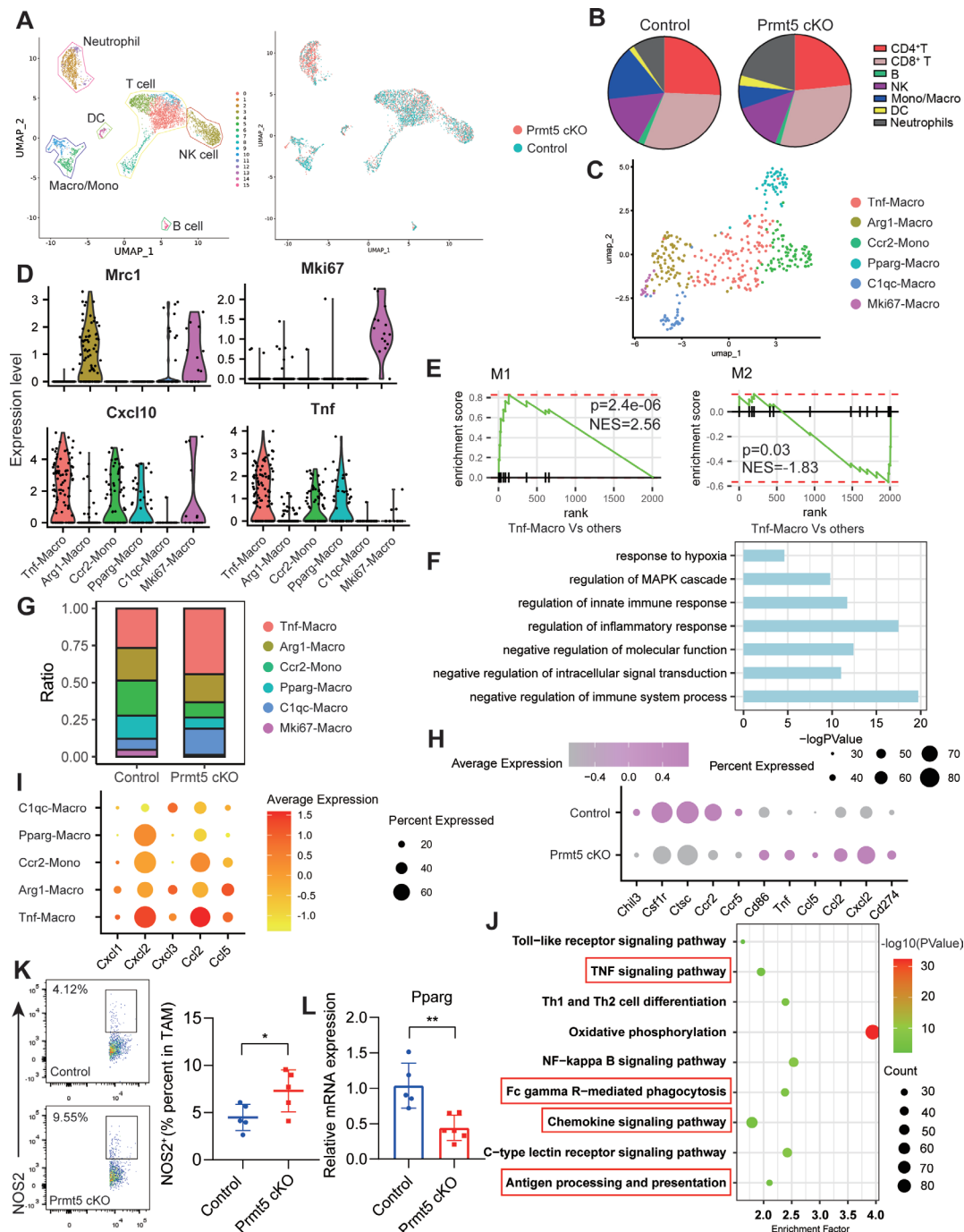


Figure 6 Deficiency of Prmt5 in myeloid cells reprogrammed macrophages and induced an antitumor phenotype in the Prmt5 cKO mice tumor. CD45⁺tumor infiltrating immune cells were isolated by FACS from the MC38 tumor bearing Prmt5 cKO and littermate control mice, and single cell RNA sequencing was performed. (A) UMAP plot showing the infiltrating immune cell clusters (left panel), colored and labeled by tissue types (right panel). (B) Pie charts of cell-type fractions between the two groups, colored by cell type. (C) UMAP plot showing the monocyte/macrophage cells re-clusters. (D) Violin plots showing the indicated gene expressions in monocyte/macrophage cell clusters. (E) Gene Set Enrichment Analysis was performed to determine the M1/M2 enriched gene signatures in Tnf-Macro cluster and the other clusters. (F) Bar graph showing the enriched terms of marker genes of Pparg-Macro cluster. (G) Percentage of each cluster in the control and Prmt5 cKO mice. (H) Dot plot showing the expression of related genes in control and Prmt5 cKO mice. (I) Dot plot showing the expression of chemokines in Mono/Macro subclusters. (J) Bubble plot of enriched KEGG pathway in tumor-infiltrating neutrophils. (K) NOS2 expression in the TAM between the control and Prmt5 cKO group measured by flow cytometry. (L) Pparg expression in TAM was determined from the control and Prmt5 cKO mice by qPCR. The mean \pm SD was graphed. Statistical differences were determined by Student's t-test (K, L), * $p < 0.05$, ** $p < 0.01$. cKO, conditional knockout; DC, dendritic cell; FACS, Fluorescence - Activated Cell Sorting; KEGG, Kyoto Encyclopedia of Genes and Genomes; mRNA, messenger RNA; NK, natural killer; PRMT5, protein arginine methyltransferase 5; TAM, tumor-associated macrophage; TNF, tumor necrosis factor; UMAP, Uniform Manifold Approximation and Projection.

Prmt5 in myeloid cells would also induce PD-L1 expression. Indeed, Cd274 (encoding PD-L1) expression was significantly elevated when Prmt5 was depleted in myeloid cells (figure 7A). This increase in PD-L1 expression was further confirmed by flow cytometry (figure 7B). Based on these findings, we hypothesized that combining myeloid cell-specific Prmt5 deletion with anti-PD-L1 antibody treatment could produce a synergistic effect, leading to improved therapeutic efficacy. As expected, tumor-bearing Prmt5 cKO mice treated with the anti-PD-L1 antibody showed significantly greater tumor growth suppression compared with control mice (figure 7C,D). Additionally, tumor-infiltrating CD3+T cells were increased in Prmt5 cKO mice treated with anti-PD-L1 antibody, while the proportion of CD25+Foxp3+ Treg cells was decreased (figure 7E,F). In addition, GZMB and IFN- γ expression in CD8+T cells was significantly elevated in Prmt5 cKO mice treated with anti-PD-L1, indicating enhanced cytotoxic activity (figure 7G). Moreover, neutrophils from the Prmt5 cKO mice treated with anti-PD-L1 showed increased expression of CD74 (figure 7H), which is consistent with the previous single-cell RNA-seq data, suggesting that these neutrophils have enhanced antigen presentation capabilities.³⁷ Our data demonstrate that ablation of Prmt5 in myeloid cells significantly enhances the efficacy of anti-PD-L1 therapy, highlighting a promising combined approach for tumor treatment.

DISCUSSION

Our study reveals a critical role for PRMT5 in the TME, particularly through its regulation of myeloid cell differentiation and macrophage polarization. While PRMT5 has previously been implicated in various oncogenic processes, and associated with poor outcomes, it has recently emerged as a potential therapeutic target in cancer and has entered clinical trials.^{14 15} However, its specific impact on myeloid cell differentiation and function has remained unclear.

First, the pan-cancer single-cell transcriptomic analysis of tumor-infiltrating myeloid cells identified high PRMT5 expression in the PPARG-macrophage subset. Elevated PRMT5 levels in these macrophages were linked to poorer survival outcomes. Using the myeloid cell-specific Prmt5 knockout mice, we demonstrated that Prmt5 is a key regulator of monocyte and macrophage differentiation, migration, and function. Deletion of Prmt5 in myeloid cells impaired monocyte-to-macrophage differentiation and macrophage migration, as evidenced by reduced proportion of monocytes in the spleen of Prmt5 cKO mice and decreased macrophage populations in thioglycolate-induced peritonitis. Additionally, Prmt5 deficiency suppressed M2 polarization in both mouse BMDMs and human monocyte-derived macrophages in vitro. PRMT5 has been identified as a regulator of cellular metabolism.³⁸ Earlier studies have shown that PRMT5 re-modulates glycolytic metabolism in pancreatic cancer and lipid metabolism in adipocytes by methylating

SREBP1a.³⁹ Similar metabolic effects have been observed in T cells, where Prmt5 promotes cholesterol biosynthesis and Th17 cell differentiation, contributing to experimental autoimmune encephalomyelitis development.⁴⁰ Consistent with these findings, our study showed that PRMT5 also affects cholesterol metabolism in macrophages. Giving the critical role of PPAR γ in M2 differentiation,⁴¹ we found that the PPARG-macrophage subset exhibited high PRMT5 expression in pan-cancer myeloid single-cell RNA-seq analysis, highlighting PRMT5's importance in M2 differentiation within the TME. In the colorectal tumor mouse model, specific deletion of Prmt5 in myeloid cells reprogrammed macrophages toward an antitumor phenotype. This shift was evidenced by a decrease in the Pparg-macrophage subset and an increase in the Tnf-macrophage subset, effectively inhibiting tumor progression. Additionally, in vitro studies of macrophage differentiation and M2 polarization confirmed that Prmt5 depletion affects lipid metabolism, identifying the pSTAT6-PPAR γ axis as a key regulatory pathway involved in M2 macrophage polarization.

Targeting PRMT5 had been a novel strategy to treat cancer and several small molecular inhibitors were in clinical trials and had preliminary results. PF-06939999 is an orally available selective inhibitor of PRMT5 and in clinical trials,¹⁴ preliminary results showed that treatment-related adverse events occurred in most of the patients, including anemia, thrombocytopenia and neutropenia, which were dose-dependent. Meanwhile, another phase I study of AMG 193, an MTA-cooperative PRMT5 inhibitor, highly selective inhibitor to treat MTAP-deleted cancer, had fewer side effects of myelosuppression.⁴² However, there were still some challenges to overcome. First, inhibition of PRMT5 may lead to a contradictory effect on tumor cells and immune cells. Therefore, it is critical to demonstrate the function of PRMT5 in different cell types in the TME to optimize the regimen of PRMT5 inhibitor treatment. Second, the potential patients who will benefit from this therapy and optimized therapeutic concentrations need to be explored in the future.

Now targeting the tumor-associated macrophages has been a new immunotherapy strategy. Previous study demonstrated that ablation of UBC9 in TAM reprograms the phenotype of macrophages and enhances CD8+T cell activation in prostate cancer.⁴³ Another study revealed that blockade of L2HGDH in TAM orchestrates macrophage polarization and inhibits tumor growth.⁴⁴ And our study demonstrated that deletion of PRMT5 reprogrammed macrophages toward an antitumor phenotype. Moreover, we found that there were overlapping properties in macrophages subset, like in Prmt5 cKO tumor-bearing mice, CD206 was downregulated but along with higher expression of PD-L1 in TAMs. The elevated PD-L1 may impair the antitumor efficacy of T cells, which might explain why the macrophage-specific knockout of Prmt5 alone does not exhibit very significant effects in the tumor model (figure 5). However, this finding provides a compelling rationale for adding PD-L1 blockade to

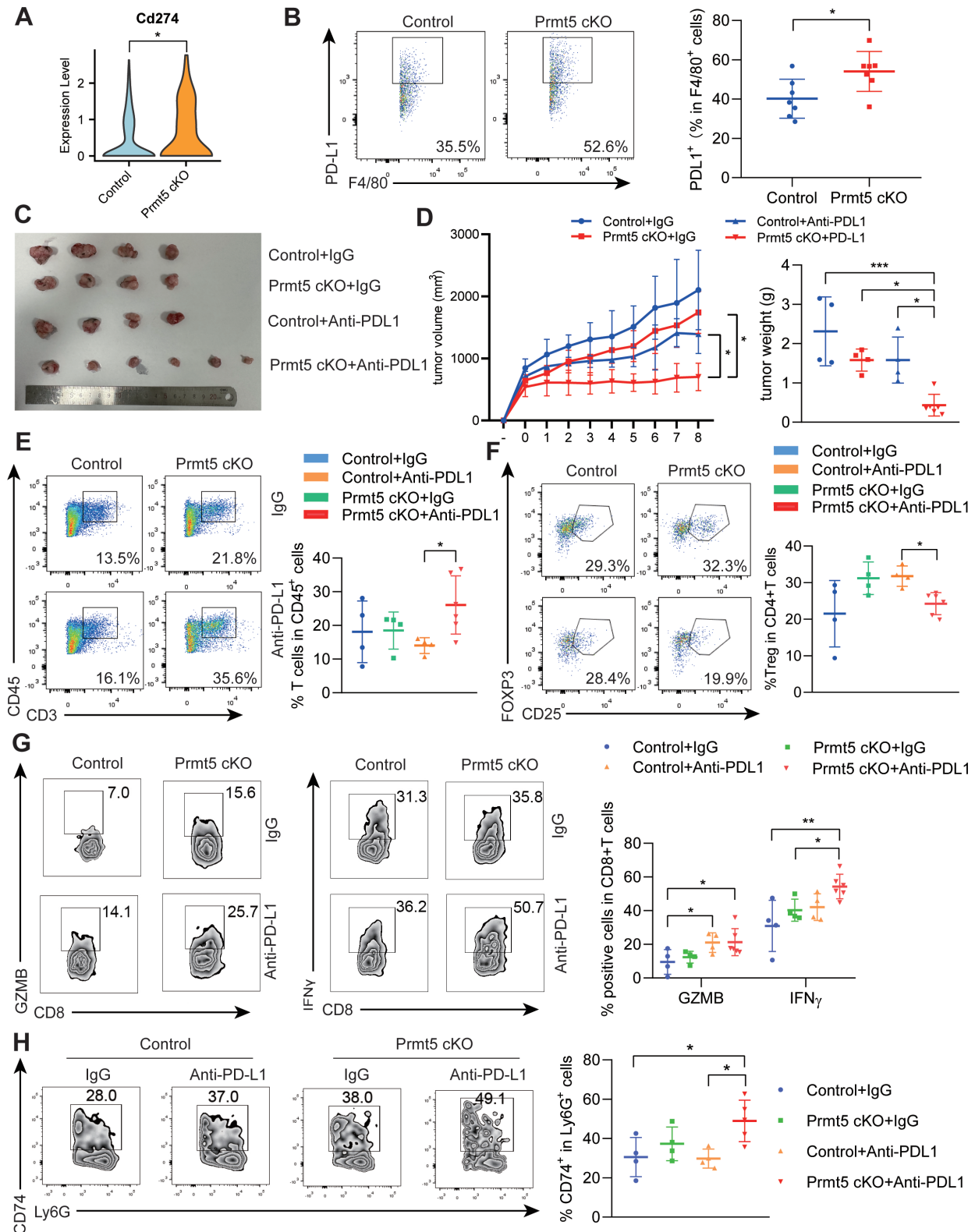


Figure 7 Anti-PD-L1 antibody synergizes with enhances antitumor ability in the Prmt5 cKO mice. (A) Violin plot showed the expression of Cd274 in monocyte/macrophage cells from control and Prmt5 cKO MC38 tumor bearing mice. (B) Tumor-associated macrophage PD-L1 expression was determined by flow cytometry from control (n=7) and Prmt5 cKO (n=7) MC38 tumor bearing mice. (C–D) Control and Prmt5 cKO mice bearing MC38 tumors were treated with IgG (10 mg/kg), anti-PD-L1 (10 mg/kg), images of resected tumor tissues (C); tumor volumes and tumor weights (D) are shown. (E–H) The percentages of tumor infiltrating CD3⁺T cells (E), CD25⁺FOXP3⁺ Treg cells (F), CD8⁺GZMB⁺, CD8⁺IFN-γ⁺ cells (G), Ly6G⁺CD74⁺ cells (H) were determined by flow cytometry from control and Prmt5 cKO MC38 tumor bearing mice. The mean±SD was graphed. Statistical differences were determined by analysis of variance test, *p<0.05, **p<0.01, ***p<0.001. cKO, conditional knockout; IFN, interferon; PD-L1, programmed death-ligand 1; PRMT5, protein arginine methyltransferase 5.

PRMT5 inhibition to enhance its therapeutic efficacy. In our mouse models, combining Prmt5 deletion with anti-PD-L1 led to substantial improvements in antitumor immunity, boosting effector T-cell function and reducing Treg populations in the TME. These changes contributed to significant tumor growth inhibition and enhanced tumor-specific immune responses. Though different tumor models present differences in the TME, like we used three different cancer cells in the mouse tumor model, while these models revealed heterogeneous immune microenvironments; prmt5 deficiency in macrophage consistently reprograms macrophages toward an antitumor phenotype and showed a consistent trend of tumor reduction.

In conclusion, our study underscores the potential of targeting PRMT5 for cancer treatment, particularly through its function in myeloid cells. We demonstrate that disrupting Prmt5 leads to metabolic changes that promote macrophages reprogramming in the TME. Moreover, our findings support the therapeutic benefit of combining Prmt5 inhibition with immune checkpoint blockade for a more effective cancer treatment strategy.

MATERIALS AND METHODS

Animal experiments

Our study examined male and female animals, and similar findings are reported for both sexes. Male and female C57BL/6 mice were purchased from the Shanghai Laboratory Animal Center, Chinese Academy of Sciences (Shanghai, China). Lysm-Cre transgenic mice were purchased from The Jackson Laboratory. Prmt5^{fl/fl} mice were obtained from the European Mutant Mouse Archive. Prmt5^{fl/fl} mice were crossed with Lysm-Cre transgenic mice to generate *Lysm-cre-Prmt5^{fl/fl}* (Prmt5 cKO) mice and Lysm-Cre-negative littermate controls (Control). The animals were housed in the animal care facilities of the Shanghai Jiao Tong University School of Medicine, Xin Hua Hospital, under pathogen-free conditions. This study was carried out in accordance with the recommendations in the guidelines. For subcutaneous tumorigenicity experiments, MC38, LLC and B16 cells (1.5×10^6 in $150 \mu\text{L}$, 50% Matrigel, Corning) were subcutaneously implanted into control and Prmt5 cKO mice, separately. For anti-PD-L1 therapy, when tumor size reached $500\text{--}1,000 \text{ mm}^3$, tumor-bearing control and Prmt5 cKO mice were injected i.p. (intraperitoneal injection) with $100 \mu\text{L}$ anti-PD-L1 antibody or IgG (10 mg/kg, Bio X Cell) as a vehicle control, IgG and anti-PD-L1 antibodies were injected intraperitoneally once every 3 days and three times in total.

Cell culture

The human acute monocytic leukemia cell line THP-1, MC38, LLC and B16 were purchased from the Cell Resource Center, Shanghai Academy of Biological Sciences. THP-1 cells and B16 cells were cultured in RPMI (Roswell Park Memorial Institute Medium) 1640 (Gibco) containing 10% (v/v) FBS (Fetal Bovine Serum)

(Gibco) and 1% penicillin/streptomycin, supplemented with β -ME (Gibco). MC38 and LLC cells were cultured in high glucose Dulbecco's Modified Eagle Medium (DMEM; Hyclone) containing 10% FBS.

Cell apoptosis analysis

Annexin V-FITC/PI Cell Apoptosis Kit (556547, BD Biosciences) was used to perform the apoptosis assay. Cell suspensions were incubated with $5 \mu\text{L}$ of annexin V and $5 \mu\text{L}$ of propidium iodide at room temperature for 15 min. The percentage of apoptosis cells was measured by flow cytometry.

Cell co-culture experiment

T cells were directly co-cultured with M0/M2 BMDMs from control and Prmt5 cKO mice with anti-CD3/CD28 treatment (anti-CD3: $1 \mu\text{g/mL}$, anti-CD28: $0.5 \mu\text{g/mL}$). After 3 days, we analyzed the percentages of T-cell subsets and T-cell cytotoxicity by flow cytometry. BMDMs and MC38 cells were co-cultured in $0.4 \mu\text{m}$ pore size transwell chambers, BMDMs were seeded on the upper chamber and MC38 cells were seeded in the lower chamber for 3 days, then cell proliferation assay was performed by CCK8 (Dojindo Laboratories, Japan). 10% CCK8 solution was added into culture medium for 1 hour at the indicated time. Cell viability was monitored by measuring the absorbance value at 450 nm.

Macrophage differentiation and treatment

Human PBMCs were isolated from healthy donors by Ficoll density centrifugation. Monocytes were isolated using CD14+MACS microbeads (Miltenyi Biotech, Germany) and then differentiated into Mo-macs in complete RPMI 1640 medium containing 10% FBS and 1% penicillin/streptomycin, in the presence of 50 ng/mL M-CSF (PeproTech) for 5 days. THP-1 cells were stimulated with 150 nM PMA (Sigma) for 48 hours and cultured with fresh complete RPMI 1640 medium for another 24 hours to differentiate into macrophages. For both monocyte-derived macrophages and THP-1-derived macrophages, 100 ng/mL LPS (Sigma) plus 50 ng/mL IFN- γ (PeproTech) were added into the culture system to generate M1 macrophages. For M2 macrophage polarization, 50 ng/mL IL-4 and 50 ng/mL IL-13 (PeproTech) were added into the culture system. Cells were harvested at the indicated time.

Bone marrow from femurs and tibias of 8–10 weeks old mice was flushed in DMEM medium and cultured in complete DMEM medium supplemented with 20 ng/mL M-CSF (PeproTech) for 5 days to generate BMDMs. Medium was replaced on day 3. BMDMs were then stimulated with 20 ng/mL IFN- γ (PeproTech) and 100 ng/mL LPS (Sigma) to generate M1 macrophages or treated with 20 ng/mL IL-4 and 20 ng/mL IL-13 (PeproTech) for 48 hours to generate M2 macrophages. To evaluate the effect of PRMT5 inhibitor GSK591 (S8111, Selleck) on macrophage polarization, M0 macrophages were treated with GSK591 ($10 \mu\text{M}$) prior to M1/M2 polarization and

added into the polarization system at the indicated time for a total of 4 days treatment. In the monocyte to macrophage differentiation experiment, GSK591 was added to the culture medium during the differentiation process.

Macrophage migration assay in vivo

1.5 mL 3% thioglycolate solution (Sigma) was injected intraperitoneally into control and Prmt5 cKO mice to induce sterile peritonitis. After 3 days induction, mice were euthanized and peritoneal cells were lavaged with 10 mL phosphate-buffered saline (PBS) and analyzed by FACS (Fluorescence - Activated Cell Sorting).

Flow cytometry analysis

For in vitro experiments, BMDMs and Mo-macs were harvested and stained with indicated antibodies at four for 30 min in the dark to detect BMDM polarization and macrophage differentiation state.

For in vivo experiments, single-cell suspensions were prepared from the blood, bone marrow, spleens, and peritoneal cavity and tumor tissues from control and Prmt5 cKO mice. Bone marrow and blood directly passed through 70 µm cell strainers after lysis of red blood cells. Spleens were extruded through a 70 µm cell strainer to obtain single-cell suspension. Tumors were dissected and minced into small pieces, then digested in RPMI 1640 complete medium containing 1 mg/mL collagenase IV (Diamond) and 0.1% DNase I (Roche) for 30 min at 37°C. Digested tissues passed through a 70 µm cell strainer to obtain single cell suspension. Peritoneal lavage collected with 10 mL PBS passed through cell strainers to obtain single cell suspensions. Obtained single cells were suspended in FACS buffer and incubated with indicated antibodies on ice in the dark for 30 min. Cells were analyzed using FACS Aria II flow cytometer (BD Biosciences). For cytokine staining, cells were stimulated with cell stimulation cocktail plus protein transport inhibitors (eBioscience) for 4 hours at 37°C. After surface staining, cells were fixed and permeabilized with the Fix/Perm Foxp3 Transcription Factor Staining Buffer Set (eBioscience) for 30 min, and then staining with indicated antibodies. Antibodies were listed in online supplemental table 1.

For isolating macrophages from spleens and tumor tissues from tumor-bearing mice, single-cell suspensions were prepared as above, and macrophages (CD11b+F4/80+) were sorted using an FACS Aria flow cytometer (BD Biosciences).

Western blotting

Cells were lysed in RIPA Lysis Buffer (Beyotime) and protein lysates were separated by SDS-PAGE (Sodium Dodecyl Sulfate - Polyacrylamide Gel Electrophoresis) and transferred to PDVF (Polyvinylidene Fluoride) membranes. Membranes were blocked by blocking buffer and then incubated with primary antibodies at four overnight, followed by incubation with secondary antibodies at room temperature. Signals were detected using the

Odyssey Infrared Imaging System. Antibodies were listed in online supplemental table 1.

Quantitative real-time PCR

Total RNA was extracted using RNeasy Mini Kit (QIAGEN) and reversed to complementary DNA (cDNA) using PrimeScript RT-PCR Kit (Takara). qPCR was performed using SYBR GREEN (Yeason) on ABI Step One Q-PCR Detection System, with b-actin/gapdh as reference control. Primers were listed in the online supplemental table 2.

Multicolor IHC (Immunohistochemistry)

Human tissue paraffin sections were provided by Xinhua Hospital, Shanghai Jiaotong University School of Medicine under an approved Institutional Review Board protocol. The paraffin sections were first placed in the 62°C paraffin oven for 1 hour before deparaffinization in xylene and then rehydrated in 100%, 95%, and 70% alcohol successively. Hydrogen peroxide blocking solution was added on sections for 10 min and then washed with PBS for three times for 5 min. Antigen was retrieved by immersion in boiling buffer (1 mmol Tris-EDTA PH=9.0) for 15 min. After washing with PBS, 5% BSA (Bovine Serum Albumin) was added to the sections for 20 min. Sections were incubated with one of the primary antibodies at 4°C overnight. After being washed by PBS for three times, sections were incubated with secondary antibodies at 37°C for 30 min. Antigenic-binding signals were amplified by TSA kit (runnertbio). The other primary antibodies were incubated successively. Images were captured by Digital Slide Scanners (PANNORAMIC SCAN II, 3D HISTECH) and analyzed by SlideViewer and ImageJ. Antibodies were listed in online supplemental table 1.

Bulk RNA-seq

BMDMs from control and Prmt5 cKO mice were prepared as shown before. Total RNA was extracted using TRIzol reagent (Invitrogen) following the manufacturer's procedure. Poly (A) RNA is purified and fragmented into small pieces, then the cleaved RNA fragments were reverse-transcribed to produce the cDNA. Fragmented DNA was selected and amplified with PCR to construct the sequencing library. Finally, we performed the 2×150bp paired-end sequencing (PE150) on an Illumina NovaSeq 6000 (LC-Bio Technology, Hangzhou, China). fastp software was used to remove the reads that contained adaptor contamination, low-quality bases and undetermined bases with default parameter and cleaned reads were mapped to the reference genome of the mouse genome (GRCm38). Gene expression was calculated by the FPKM (Fragments Per Kilobase of transcript per Million mapped reads) method.

Single-cell sequencing

MC38 tumors from control and Prmt5 cKO mice were extracted and digested to obtain single-cell suspensions. Tumor infiltrating CD45+ cells were isolated by flow

cytometry and were concentrated to 800–1,000 cells/ μ L and loaded on Chromium Single Cell Controller (10x Genomics) to generate single-cell gel beads in the emulsion. The libraries were generated using the 10x Genomics Chromium Controller Instrument and Chromium Single Cell 3' V3 Reagent Kits (10x Genomics, Pleasanton, California, USA) according to the manufactures' protocol and sequencing on an Illumina sequencer (Illumina, San Diego, California, USA) in a 150 bp paired-end run.

Single-cell RNA analysis

Cell Ranger was used to process raw data. Genes with low detected cell numbers and cells with fewer than 200 genes were excluded. Meanwhile, cells were also removed if their proportions of mitochondrial gene expression >20%. The remaining 6,969 cells were used in downstream analysis. The Seurat Package was used for cell normalization and regression to obtain the scaled barcode-gene matrix. The top 2,000 variable genes were identified and used for principal component analysis. The top 10 PCA (Principal Component Analysis) were used in the FindNeighbors function and UMAP (Uniform Manifold Approximation and Projection) construction. The FindClusters function was used to identify cell clusters and clusters were visualized with UMAP plots. We calculated the cluster marker genes using the FindAllMarkers function. At this step, we remove non-immune cells that were introduced during sorting and low-quality cells. Then, we performed the unsupervised clustering algorithm again, using the top 15 PCA components. Finally, we identified six main cell types. To identify subsets in myeloid cells and T cells, we further performed unsupervised clustering in indicated cells identified in CD45+ cells.

Functional enrichment analysis

GSEA analysis for sc-RNA-seq (Single - cell RNA sequencing) was performed to identify different expression patterns in gene sets in the Gene Ontology knowledge base between Mono/Macro subset from control and Prmt5 cKO mice. We used the FindMarkers function to identify the different expression genes between TAMs from control and Prmt5 cKO tumor-bearing mice. GO terms were downloaded in the MSigDB database. GSEA analysis for bulk RNA-seq in BMDMs was performed on GSEA software. TAM M1/M2 gene sets were listed in online supplemental table 3.

TCGA database and survival analysis

Survival analyses were performed using the GEPIA Webserver (<http://gepia2.cancer-pku.cn/>). P values were calculated using Kaplan-Meier methods with a log-rank test.

Analysis of public sc-RNA-seq data

Published pan-cancer infiltrating myeloid cells single-cell transcriptomic data were downloaded from the Gene Expression Omnibus database (GSE154763). Gene expression and cell annotation was downloading from (<http://panmyeloid.cancer-pku.cn/>).

Statistical analysis

Statistical analysis was performed on Prism V.8 (GraphPad Software) and presented as mean \pm SD. The Student's unpaired two-tailed t-test was used for comparisons between two groups, analysis of variance test was used for comparisons of more than two groups. Statistical significance was denoted with (* p <0.05; ** p <0.01; *** p <0.001) in the figures. Survival analysis was estimated by the Kaplan-Meier method and compared by log-rank tests.

Study approval

Clinical samples were collected from the Xinhua Hospital, Shanghai Jiaotong University School of Medicine. Prior to participation, written informed consent was obtained from all subjects. All studies were performed in accordance with the Declaration of Helsinki. The study was approved by the Research Ethics Board of the Xinhua Hospitals, Shanghai Jiao Tong University School of Medicine, ethical number: XHEC-NSFC-2023–277.

Data and code availability

Underlying data and supporting analytic code for the article are available upon reasonable request.

Author affiliations

¹Department of Laboratory Medicine, Xin Hua Hospital, Shanghai Jiao Tong University School of Medicine, Shanghai, People's Republic of China

²Faculty of Medical Laboratory Science, Shanghai Jiao Tong University School of Medicine, Shanghai, People's Republic of China

³Institute of Artificial Intelligence Medicine, Shanghai Academy of Experimental Medicine, Shanghai, People's Republic of China

⁴Rutgers Cancer Institute of New Jersey, New Brunswick, New Jersey, USA

⁵Medicine, Rutgers Robert Wood Johnson Medical School, New Brunswick, New Jersey, USA

Contributors YZ, LS, and JC designed experiments. ZC, BZ, YC, YH, and QP performed the experiments. YZ and SC analyzed data. YZ, SC, LS, and JC wrote the manuscript, and all authors contributed to the writing and providing feedback. YZ is the guarantor of this work.

Funding This work was supported by grants from the National Natural Science Foundation of China (82371738 and 82071753 to YZ), Shanghai Natural Science Foundation (23ZR1441700 to YZ), and Shanghai Municipal Health Commission of Outstanding Youth Talent Program (20224Z0025 to YZ).

Competing interests None declared.

Patient consent for publication Not applicable.

Ethics approval Not applicable.

Provenance and peer review Not commissioned; externally peer reviewed.

Data availability statement Data are available upon reasonable request.

Supplemental material This content has been supplied by the author(s). It has not been vetted by BMJ Publishing Group Limited (BMJ) and may not have been peer-reviewed. Any opinions or recommendations discussed are solely those of the author(s) and are not endorsed by BMJ. BMJ disclaims all liability and responsibility arising from any reliance placed on the content. Where the content includes any translated material, BMJ does not warrant the accuracy and reliability of the translations (including but not limited to local regulations, clinical guidelines, terminology, drug names and drug dosages), and is not responsible for any error and/or omissions arising from translation and adaptation or otherwise.

Open access This is an open access article distributed in accordance with the Creative Commons Attribution Non Commercial (CC BY-NC 4.0) license, which permits others to distribute, remix, adapt, build upon this work non-commercially, and license their derivative works on different terms, provided the original work is properly cited, appropriate credit is given, any changes made indicated, and the use is non-commercial. See <http://creativecommons.org/licenses/by-nc/4.0/>.

ORCID iDs

Shiyu Chen <http://orcid.org/0009-0002-1309-0175>
 Zheyi Chen <http://orcid.org/0009-0007-1809-5043>
 Bingqian Zhou <http://orcid.org/0009-0008-3309-6615>
 Yongyu Chen <http://orcid.org/0009-0009-2260-9718>
 Yiren Huang <http://orcid.org/0009-0006-0192-9163>
 Jian Cao <http://orcid.org/0000-0003-3424-6802>
 Lisong Shen <http://orcid.org/0000-0002-6647-4749>
 Yingxia Zheng <http://orcid.org/0000-0002-8074-0716>

REFERENCES

- Bedford MT, Clarke SG. Protein arginine methylation in mammals: who, what, and why. *Mol Cell* 2009;33:1–13.
- Radziszewska A, Shliha PV, Grinev V, et al. PRMT5 methylome profiling uncovers a direct link to splicing regulation in acute myeloid leukemia. *Nat Struct Mol Biol* 2019;26:999–1012.
- Yang L, Ma D-W, Cao Y-P, et al. PRMT5 functionally associates with EZH2 to promote colorectal cancer progression through epigenetically repressing CDKN2B expression. *Theranostics* 2021;11:3742–59.
- Li W-J, He Y-H, Yang J-J, et al. Profiling PRMT methylome reveals roles of hnRNP1 arginine methylation in RNA splicing and cell growth. *Nat Commun* 2021;12:1946.
- Scoumanne A, Zhang J, Chen X. PRMT5 is required for cell-cycle progression and p53 tumor suppressor function. *Nucleic Acids Res* 2009;37:4965–76.
- Pastore F, Bhagwat N, Pastore A, et al. PRMT5 Inhibition Modulates E2F1 Methylation and Gene-Regulatory Networks Leading to Therapeutic Efficacy in JAK2^{V617F}-Mutant MPN. *Cancer Discov* 2020;10:1742–57.
- Zheng Y, Huang L, Ge W, et al. Protein Arginine Methyltransferase 5 Inhibition Upregulates Foxp3⁺ Regulatory T Cells Frequency and Function during the Ulcerative Colitis. *Front Immunol* 2017;8:596.
- Gullà A, Hideshima T, Bianchi G, et al. Protein arginine methyltransferase 5 has prognostic relevance and is a druggable target in multiple myeloma. *Leukemia* 2018;32:996–1002.
- Quan X, Yue W, Luo Y, et al. The protein arginine methyltransferase PRMT5 regulates Aβ-induced toxicity in human cells and Caenorhabditis elegans models of Alzheimer's disease. *J Neurochem* 2015;134:969–77.
- Zheng Y, Chen Z, Zhou B, et al. Prmt5 deficiency inhibits CD4⁺ T-cell Klf2/S1pr1 expression and ameliorates EAE disease. *J Neuroinflammation* 2023;20:183.
- Zhu F, Guo H, Bates PD, et al. PRMT5 is upregulated by B-cell receptor signaling and forms a positive-feedback loop with PI3K/AKT in lymphoma cells. *Leukemia* 2019;33:2898–911.
- Sheng X, Bowen N, Wang Z. GLI pathogenesis-related 1 functions as a tumor-suppressor in lung cancer. *Mol Cancer* 2016;15:25.
- Rengasamy M, Zhang F, Vashisht A, et al. The PRMT5/WD77 complex regulates alternative splicing through ZNF326 in breast cancer. *Nucleic Acids Res* 2017;45:11106–20.
- Rodon J, Rodriguez E, Maitland ML, et al. A phase I study to evaluate the safety, pharmacokinetics, and pharmacodynamics of PF-06939999 (PRMT5 inhibitor) in patients with selected advanced or metastatic tumors with high incidence of splicing factor gene mutations. *ESMO Open* 2024;9:102961.
- Vieito M, Moreno V, Spreafico A, et al. Phase 1 Study of JNJ-64619178, a Protein Arginine Methyltransferase 5 Inhibitor, in Advanced Solid Tumors. *Clin Cancer Res* 2023;29:3592–602.
- Engstrom LD, Aranda R, Waters L, et al. MRTX1719 Is an MTA-Cooperative PRMT5 Inhibitor That Exhibits Synthetic Lethality in Preclinical Models and Patients with MTAP-Deleted Cancer. *Cancer Discov* 2023;13:2412–31.
- Belmontes B, Slemmons KK, Su C, et al. AMG 193, a Clinical Stage MTA-Cooperative PRMT5 Inhibitor, Drives Antitumor Activity Preclinically and in Patients with MTAP-Deleted Cancers. *Cancer Discov* 2025;15:139–61.
- Zheng Y, Chen Z, Zhou B, et al. PRMT5 Deficiency Enforces the Transcriptional and Epigenetic Programs of Klr1⁺CD8⁺ Terminal Effector T Cells and Promotes Cancer Development. *J Immunol* 2022;208:501–13.
- Zhou B, Chen N, Chen Z, et al. Prmt5 deficient mouse B cells display RNA processing complexity and slower colorectal tumor progression. *Eur J Immunol* 2023;53:e2250226.
- Jakubczik CV, Randolph GJ, Henson PM. Monocyte differentiation and antigen-presenting functions. *Nat Rev Immunol* 2017;17:349–62.
- Guilliams M, Mildner A, Yona S. Developmental and Functional Heterogeneity of Monocytes. *Immunity* 2018;49:595–613.
- Huang B, Lei Z, Zhao J, et al. CCL2/CCR2 pathway mediates recruitment of myeloid suppressor cells to cancers. *Cancer Lett* 2007;252:86–92.
- Zaslona Z, Serezani CH, Okunishi K, et al. Prostaglandin E2 restrains macrophage maturation via E prostanoic receptor 2/protein kinase A signaling. *Blood* 2012;119:2358–67.
- Silva LM, Lum AG, Tran C, et al. Plasmin-mediated fibrinolysis enables macrophage migration in a murine model of inflammation. *Blood* 2019;134:291–303.
- Tae S, Karkhanis V, Velasco K, et al. Bromodomain protein 7 interacts with PRMT5 and PRC2, and is involved in transcriptional repression of their target genes. *Nucleic Acids Res* 2011;39:5424–38.
- Liu M, Yao B, Gui T, et al. PRMT5-dependent transcriptional repression of c-Myc target genes promotes gastric cancer progression. *Theranostics* 2020;10:4437–52.
- Huang SC-C, Everts B, Ivanova Y, et al. Cell-intrinsic lysosomal lipolysis is essential for alternative activation of macrophages. *Nat Immunol* 2014;15:846–55.
- Goossens P, Rodriguez-Vita J, Etzerodt A, et al. Membrane Cholesterol Efflux Drives Tumor-Associated Macrophage Reprogramming and Tumor Progression. *Cell Metab* 2019;29:1376–89.
- Lee CH, Evans RM. Peroxisome proliferator-activated receptor-gamma in macrophage lipid homeostasis. *Trends Endocrinol Metab* 2002;13:331–5.
- Tang W, Sun G, Ji G-W, et al. Single-cell RNA-sequencing atlas reveals an FABP1-dependent immunosuppressive environment in hepatocellular carcinoma. *J Immunother Cancer* 2023;11:e007030.
- Gopalakrishnan A, Joseph J, Shirey KA, et al. Protection against influenza-induced Acute Lung Injury (ALI) by enhanced induction of M2a macrophages: possible role of PPARγ/RXR ligands in IL-4-induced M2a macrophage differentiation. *Front Immunol* 2022;13:968336.
- Isali I, McClellan P, Shankar E, et al. Genipin guides and sustains the polarization of macrophages to the pro-regenerative M2 subtype via activation of the pSTAT6-PPAR-gamma pathway. *Acta Biomater* 2021;131:198–210.
- Rao L-Z, Wang Y, Zhang L, et al. IL-24 deficiency protects mice against bleomycin-induced pulmonary fibrosis by repressing IL-4-induced M2 program in macrophages. *Cell Death Differ* 2021;28:1270–83.
- Giese MA, Hind LE, Huttenlocher A. Neutrophil plasticity in the tumor microenvironment. *Blood* 2019;133:2159–67.
- Orecchioni M, Ghosheh Y, Pramod AB, et al. Macrophage Polarization: Different Gene Signatures in M1(LPS+) vs. Classically and M2(LPS-) vs. Alternatively Activated Macrophages. *Front Immunol* 2019;10:1084.
- Hu R, Zhou B, Chen Z, et al. PRMT5 Inhibition Promotes PD-L1 Expression and Immuno-Resistance in Lung Cancer. *Front Immunol* 2021;12:722188.
- Wu Y, Ma J, Yang X, et al. Neutrophil profiling illuminates anti-tumor antigen-presenting potency. *Cell* 2024;187:1422–39.
- Mavrikis KJ, McDonald ER, Schlachet MR, et al. Disordered methionine metabolism in MTAP/CDKN2A-deleted cancers leads to dependence on PRMT5. *Science* 2016;351:1208–13.
- Liu L, Zhao X, Zhao L, et al. Arginine Methylation of SREBP1a via PRMT5 Promotes De Novo Lipogenesis and Tumor Growth. *Cancer Res* 2016;76:1260–72.
- Webb LM, Sengupta S, Edell C, et al. Protein arginine methyltransferase 5 promotes cholesterol biosynthesis-mediated Th17 responses and autoimmunity. *J Clin Invest* 2020;130:1683–98.
- Odegaard JI, Ricardo-Gonzalez RR, Goforth MH, et al. Macrophage-specific PPARgamma controls alternative activation and improves insulin resistance. *Nature New Biol* 2007;447:1116–20.
- Rodon J, Prenen H, Sacher A, et al. First-in-human study of AMG 193, an MTA-cooperative PRMT5 inhibitor, in patients with MTAP-deleted solid tumors: results from phase I dose exploration. *Ann Oncol* 2024;35:1138–47.
- Xiao J, Sun F, Wang Y-N, et al. UBC9 deficiency enhances immunostimulatory macrophage activation and subsequent antitumor T cell response in prostate cancer. *J Clin Invest* 2023;133:e158352.
- Feng S, Wang D, Jin Y, et al. Blockage of L2HGDH-mediated S-2HG catabolism orchestrates macrophage polarization to elicit antitumor immunity. *Cell Rep* 2024;43:114300.